ELSEVIER

0263-8223(95)00083-6

Composite Structures 32 (1995) 255–264

0263-8223/95/$9.50

Finite element procedure for modelling fibre metal laminates

F. Hashagen, J. C. J. Schellekens, R. de Borst*

Department of Civil Engineering, Delft University of Technology, PO 5048, 2600 GA Delft, The Netherlands

&

H. Parisch

Institute for Statics and Dynamics of Aerospace Structures, University of Stuttgart, Pfaffenwaldring 27, 70550 Stuttgart, Germany

A geometrically and physically nonlinear solid-like shell element is presented to analyse the behaviour of laminated structures. The geometrically nonlinear formulation of the element is derived from three-dimensional continuum mechanics and accounts for the change of thickness. The geometry of the element is described by sixteen nodes which are located at the top and the bottom surface of the element. At each node three translational degrees of freedom are defined. Additionally, four internal degrees of freedom are assumed to improve the description of the internal stretching. The physically nonlinear behaviour is assumed to be governed by the Hoffmann yield criterion for orthotropic materials and the von Mises yield criterion for isotropic materials. It is explained how the element can be applied to laminated structures. By calculating benchmark tests obtained from the literature the behaviour of the element is compared with that of standard finite shell and solid elements. From these tests it is concluded that the solid-like shell element is well suited to compute laminated structures. Finally, the element is applied to compute the behaviour of a tensile specimen made of the Fibre Metal Laminate GLARE® which gives results which are in good agreement with experimental data.

1 INTRODUCTION

The economical situation of commercially operating airlines is characterized by an increasing pressure on the direct operation costs due to an ever increasing worldwide competition. Since the price for flying is decreasing, the number of passengers shipped has increased which results in an overload of the existing infrastructure due to an increasing number of flights. To reduce the operation costs or to lift the number of passengers per flight new aircraft designs have to be taken into consideration. This leads to incremental improvement of existing flight vehicles or to the development of a new aircraft generation which is discussed as 'Super-Jumbo'. To achieve a design concept which reaches this target intensive research in the fields of avionics, propulsion technologies and aerodynamics is undertaken. Another field which offers a great potential for the improvement of the design concepts is the structure of the aircraft. Here the application of new materials offers improvements resulting from the material properties itself, but also from the improvement of existing structural design concepts. In consideration of this potential the Fibre Metal Laminates (FML) ARALL® and GLARE® have been developed at the Production and Materials Laboratory of the Faculty of Aerospace Engineering of Delft University of Technology. The materials are characterized by aluminium layers (alu. 2024-T3, alu. 7075-T6)

*Also at: Department of Mechanical Engineering, Eindhoven University of Technology, PO Box 513, 5600 GA Eindhoven, Netherlands.

which are connected to each other by either R-Glass or Aramid prepreg layers. In general, an unlimited number of aluminium layers could be connected to each other by prepreg layers. ARALL® and GLARE® are composed of three aluminium layers connected by two prepreg layers. The potential of weight saving is between 20–30% compared with structures built using aluminium alloys. In relation to other advanced composites the relative costs are forecasted to be halved.[1]

To make full use of these advanced materials proper design concepts and reliable computational methods are necessary. These methods have to describe effects caused by the interlaminar reaction, the various failure mechanisms and geometrical nonlinearities. As part of this research project structural parts of an aircraft shall be modelled with finite elements. These parts typically occur in huge thin-walled structures. When applying standard finite elements to these problems, proper modelling leads to difficulties. On the one hand standard solid elements tend to lock for large length/thickness ratios. To avoid this locking phenomenon a finite element model applying a large number of elements has to be used, which leads to considerable calculation time. Since the topology of standard shell elements is reduced to the location of the nodal points on the mid-surface the application of standard shell elements leads to problems when modelling interlaminar effects in a three-dimensional state. To avoid numerical difficulties on one hand and to account for the various failure effects on the other hand a solid-like shell element is applied.

In the literature several methods are described for a solid-like shell element. In contrast to the element used here most solid-like elements account for the change of thickness via a staggered iterative update procedure which is constructed by exploiting the plane-stress assumption. Simo *et al.*[2] present an approach in which the thickness director is a truly independent field which is coupled with bending, membrane and transverse shear fields through the constitutive equation. The method introduced by Büchter *et al.*[3] applies the enhanced natural strain concept to obtain a three-dimensional constitutive relation. Assuming a linearly varying thickness director the displacement field is separated into the displacement field of the mid-surface and the displacement of the thickness director. Due to this separation in the latter two cases the finite elements cannot simply be coupled in thickness direction with other elements which is disadvantageous when modelling interlaminar effects in layered materials.

For these reasons a solid-like shell element is used, which is based on a three-dimensional continuum theory with sixteen geometrical nodes as proposed by Parisch.[4] Hereby three translational degrees of freedom are defined at each node, Fig. 1. Additionally, four internal degrees of freedom are established at the corners of the element to account for the internal stretching, which yields a fully three-dimensional field of membrane and bending strains. Accordingly, these solid-like shell elements can be coupled in thickness direction in a straight forward manner, which is advantageous when modelling interlaminar effects in a three-dimensional state. Furthermore, locking effects that occur with standard solid elements are avoided.

2 ELEMENT GEOMETRY AND KINEMATICS

Using the Green strain tensor γ which is defined as:

$$\gamma=\frac{1}{2}(f^{\mathrm{T}}f-F^{\mathrm{T}}F); \tag{1}$$

the strains are calculated by expressing the deformation tensor F in the undeformed configuration and the deformation tensor f in the deformed configuration in terms of the corresponding metric vectors $\mathbf{G}_i$ and $\mathbf{g}_i$.[4,5] The latter quantities are derived from the derivatives of the position vector of an arbitrary material point P in the deformed state $\mathbf{x}$ and the undeformed state $\mathbf{X}$ in the element with respect to the isoparametric coordinates $\Theta^i=\{\xi,\eta,\zeta\}$.

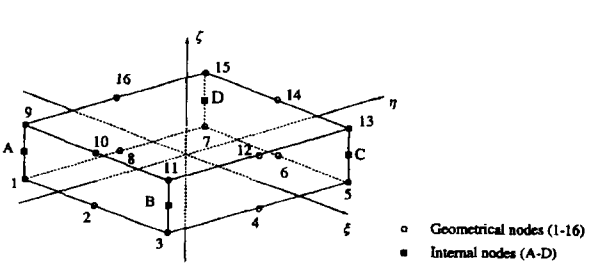

Fig. 1. Element geometry and nodes of the sixteen-noded solid-like shell element.

Denoting the displacement vector of the mid-surface as $\mathbf{u}^0$, the change of thickness as $\mathbf{u}^1$ and the internal stretching as $\mathbf{u}^2$, the displacement field at point P is written as:

$$\mathbf{u}=\mathbf{u}^0+\zeta\mathbf{u}^1+(1-\zeta^2)\mathbf{u}^2, \tag{2}$$

which yields for the position of P in the deformed configuration:

$$\mathbf{x}=\mathbf{X}+\mathbf{u}. \tag{3}$$

By specifying the classical kinematics of rigid rotation of the shell director the description of the internal stretching is reduced to one parameter w_3. Accordingly, we get for the corresponding displacement vector $\mathbf{u}^2=w_3\mathbf{d}$, where $\mathbf{d}$ denotes the director in the deformed state. By invoking the internal stretching a fully three-dimensional strain field is described. In a global iteration procedure the equations characterizing the equilibrium are solved for the change of displacements. After computing the metric vector and subsequently the deformation tensors, the change of the Green strains within an iteration j can be derived as:[5]

$$\begin{aligned} d\gamma^G=&(d\varepsilon_{\alpha\beta}+\zeta\, d\rho_{\alpha\beta})\mathbf{E}^\alpha\otimes\mathbf{E}^\beta\\ &+(d\varepsilon_{\alpha 3}+\zeta\, d\rho_{\alpha 3})\mathbf{E}^\alpha\otimes\mathbf{E}^3\\ &+(d\varepsilon_{3\alpha}+\zeta\, d\rho_{3\alpha})\mathbf{E}^3\otimes\mathbf{E}^\alpha\\ &+(d\varepsilon_{33}+\zeta\, d\rho_{33})\mathbf{E}^3\otimes\mathbf{E}^3. \end{aligned} \tag{4}$$

Here the strains are decomposed into a ζ-independent membrane part and a ζ-dependent bending part $d\varepsilon_{kl}$ and $d\rho_{kl}$, respectively. The contravariant vector $\mathbf{E}^\alpha$ is calculated[4,5] using the covariant metric vector $\mathbf{E}_\alpha$ which is defined by using the position of the mid-surface $\mathbf{X}^0$.

$$\mathbf{E}_\alpha=\frac{\partial\mathbf{X}^0}{\partial\Theta^\alpha},\ \text{with}\ \alpha,\beta=1,2.$$

Performing the substitution of the deformation tensors in eqn (1) and decomposing the strains according to eqn (4) into the membrane and bending components the following expressions can be derived:

$$2d\varepsilon_{\alpha\beta}=e_\beta.d\mathbf{u}^0_{,\alpha}+e_\alpha.d\mathbf{u}^0_{,\beta}+d\mathbf{u}^0_{,\alpha}.d\mathbf{u}^0_{,\beta}, \tag{5}$$

$$2d\varepsilon_{\alpha 3}=e_\alpha.d\mathbf{u}^1+\mathbf{d}.d\mathbf{u}^0_{,\alpha}+d\mathbf{u}^0_{,\alpha}.d\mathbf{u}^1, \tag{6}$$

$$2d\varepsilon_{33}=2\mathbf{d}.d\mathbf{u}^1+2d\mathbf{u}^1.d\mathbf{u}^1, \tag{7}$$

$$\begin{aligned} 2d\rho_{\alpha\beta}=&e_\beta.d\mathbf{u}^1_{,\alpha}+\mathbf{d}_{,\alpha}d\mathbf{u}^0_{,\beta}+d\mathbf{u}^1_{,\alpha}.d\mathbf{u}^0_{,\beta}\\ &+e_{,\alpha}.d\mathbf{u}^1_{,\beta}+\mathbf{d}_{,\beta}.d\mathbf{u}^0_{,\alpha}+d\mathbf{u}^1_{,\beta}.d\mathbf{u}^0_{,\alpha}\\ &-(e_\lambda.d\mathbf{u}^0_{,\beta}+e_\beta.d\mathbf{u}^0_{,\lambda}+d\mathbf{u}^0_{,\lambda}.d\mathbf{u}^0_{,\beta})\bar{G}^\lambda_\alpha\\ &-(e_\alpha.d\mathbf{u}^0_{,\tau}+e_\tau.d\mathbf{u}^0_{,\alpha}+d\mathbf{u}^0_{,\alpha}.d\mathbf{u}^0_{,\tau})\bar{G}^\tau_\beta, \end{aligned} \tag{8}$$

$$2d\rho_{\alpha 3}=\mathbf{d}_{,\alpha}.d\mathbf{u}^1+\mathbf{d}.d\mathbf{u}^1_{,\alpha}+d\mathbf{u}^1_{,\alpha}.d\mathbf{u}^1, \tag{9}$$

$$\begin{aligned} 2d\rho_{33}=&-8w_3\mathbf{d}.d\mathbf{u}^1-4\mathbf{d}.\mathbf{d}dw_3\\ &-4dw_3\mathbf{d}.d\mathbf{u}^1-4w_3d\mathbf{u}^1.d\mathbf{u}^1. \end{aligned} \tag{10}$$

The quantity e_α denotes the derivative of the shell mid-surface in the deformed configuration $\mathbf{x}^0$ with respect to the isoparametric coordinates, ξ and η. Applying G^i_j the mixed-variant metric is introduced which can be computed using the constant part of the contravariant metric G^{0jm} and the linear part of the covariant metric G^1_{mk}.[5] The strains defined by eqns (5)–(10) are calculated with respect to the in general non-orthogonal reference system $\mathbf{E}^j$. However, for composite materials the stress–strain relation is conveniently accomplished in a local frame $\mathbf{m}_j$ which is provided by the characteristic material directions. The change of strains in the material system $d\gamma_{ij}$ is derived by applying the transformation t^k_i from the reference system $\mathbf{E}^k$ to the local system $\mathbf{m}_i$:

$$d\gamma_{ij}=(d\varepsilon_{kl}+\zeta d\rho_{kl})t^k_i t^l_j,\ \text{with}\ t^k_i=(\mathbf{E}^k.\mathbf{m}_i).$$

To set up the stiffness matrices the tensor $d\gamma_{ij}$ can be rewritten using vector-matrix notation. The strains depend on the displacement $\mathbf{u}$ and its derivatives with respect to the isoparametric coordinates. If the displacements are arranged in the following manner:

$$d\mathbf{z}=(d\mathbf{u}^0,d\mathbf{u}^1,dw_3)^{\mathrm{T}},$$

then the change of the strains can be decomposed into a linear part $d\gamma^L$ and a nonlinear part $d\gamma^{NL}$.[4,5] The displacements $d\mathbf{u}^0$, $d\mathbf{u}^1$ and dw_3 are expressed in terms of nodal displacements and their corresponding shape functions. To achieve this approximation the nodal displacements of the sixteen nodes and the four internal nodes are arranged in the following way:

$$\begin{aligned} d\hat{\mathbf{u}}^T=&(du^1_x,\ldots,du^{16}_x,du^1_y,\ldots,du^{16}_y,du^1_z,\\ &\ldots,du^{16}_z,dw^A_3,\ldots,dw^D_3). \end{aligned} \tag{11}$$

Using the vector of nodal displacements and the shape functions the vector $d\mathbf{z}$ is written as:[5]

$$d\mathbf{z}=\begin{bmatrix}\mathrm{diag}(\Pi^0) & 0\\ \mathrm{diag}(\Pi^1) & 0\\ 0^T & \Pi^w\end{bmatrix} d\hat{\mathbf{u}}=\Lambda\, d\hat{\mathbf{u}}. \tag{12}$$

The matrices Π^0, Π^1 and Π^w contain the shape functions. They are derived from the ordinary isoparametric shape functions of an eight-noded standard shell element.[5] Employing the approximation by shape functions and nodal values the linear part $d\gamma^L$ can be written as:[5]

$$d\gamma^L = \mathbf{B}_L \, d\hat{\mathbf{u}}. \tag{13}$$

The matrix $\mathbf{B}_L$ contains the derivatives of the displacements, the approximation with shape functions and the transformation into the material frame of reference.[5] Accordingly, eqn (13) relates the nodal displacements to the strains with respect to the material system. In principle the derivation of the nonlinear part is achieved in the same way. But a vector of nonlinear strains cannot as conveniently be composed as for the linear part. Therefore, the derivation of the nonlinear strains is performed for each component separately. When calculating the nonlinear contribution to the stiffness matrix this leads to a sum of different matrices representing the shape functions, their derivatives and transformations.[5]

3 THE STIFFNESS MATRICES

The derivation of the stiffness matrices is based on the weak form of the equilibrium equations.[4] While integrating the equations over the volume special attention has to be paid to the integration in thickness direction. Since the element may consist of different layers with varying material properties the integration in thickness direction is split up in a number of n_L subintegrations. Hereby n_L denotes the number of layers. For every layer the constitutive relation is built with the individual material parameters represented by the matrix $\mathbf{D}_i$. Assuming a total Lagrangian formulation the equilibrium is established as:

$$\begin{aligned} &\sum_{i=1}^{n_L} \int_{V_{0i}} \delta(d\gamma^L)^T \mathbf{D}_i (d\gamma^L) \, dV_{0i} \\ &\quad + \sum_{i=1}^{n_L} \int_{V_{0i}} \delta(d\gamma^{NL})^T \sigma_i \, dV_{0i} \\ &\quad = \delta(d\mathbf{u})^T \mathbf{f}_{ex} - \sum_{i=1}^{n_L} \int_{V_{0i}} \delta(d\gamma^L)^T \sigma_i \, dV_{0i}. \end{aligned} \tag{14}$$

Substituting the expressions for the linear parts of the strains, eqn (13), and those for the nonlinear parts the equilibrium is described with terms up the order three in the displacement increment. By linearizing the equilibrium equations and accomplishing the integration over the volume the following system of equations is reached which must be solved for the change of displacements in iteration j:[5]

$$(\mathbf{K}_L^j + \mathbf{K}_{NL}^j) d\mathbf{u}^{j+1} = \mathbf{f}_{ex}^j - \mathbf{f}_{in}^j. \tag{15}$$

The matrix $\mathbf{K}_L$ denotes the contribution of the linear part and is computed performing a triple matrix multiplication of the constitutive matrix $\mathbf{D}_i$ and the matrix $\mathbf{B}$. The matrix $\mathbf{K}_{NL}$ denotes the nonlinear contribution to the total stiffness matrix and represents a sum of the nonlinear strains multiplied with the corresponding stresses. To obtain the element stiffness matrix the internal degrees of freedom are condensed on element level. For a detailed description of the derivation of the element stiffness matrices the reader is referred to Parisch[4] or Hashagen.[5] The element matrices can therefore be assembled to the total structural stiffness matrices. The resulting system of equations is solved using an arc-length controlled procedure.[6]

4 PHYSICALLY NONLINEAR BEHAVIOUR

Since the structures composed of composite materials show local failure effects the constitutive equations describing the stress–strain relation on local level have to be refined. An advantage of the present shell formulation is that standard three-dimensional constitutive models can be applied. Since fibre metal laminates consist of aluminium layers and of prepreg layers two different kinds of constitutive models shall be used here. The aluminium layer can be described by the isotropic von Mises yield criterion. Accordingly, the orthotropy caused by producing the aluminium layers is neglected. The yield function $\Phi(\sigma)$ which signals the onset of plastic behaviour then equals:[7]

$$\Phi(\sigma) = \sqrt{3/2 \sigma^T \mathbf{P} \sigma} - \bar{\sigma}, \tag{16}$$

where the yield value $\bar{\sigma}$ can be measured from a uniaxial tension test. The matrix $\mathbf{P}$ denotes a projection matrix with constant components.[7] However, the prepreg layers are considered to behave as orthotropic material and the von Mises yield criterion does not describe this behaviour. Accordingly, the Hoffmann yield criterion[8] is applied to the prepreg layers. The Hoffmann yield criterion is a modification of

the Hill yield criterion,[9] such that by inclusion of terms varying linearly in the stress, differences between the tensile and the compression properties can be described. The Hoffmann yield criterion is written as:[10]

$$\Phi(\sigma)=\frac{1}{2}\sigma^T\mathbf{P}_\alpha\sigma+\mathbf{p}_\alpha\sigma-\bar{\sigma}. \tag{17}$$

The matrix $\mathbf{P}_\alpha$ in eqn (17) contains six parameters which can be obtained from six uniaxial tension and compression tests. The vector $\mathbf{p}_\alpha$ contains three additional parameters and $\bar{\sigma}$ denotes the normalized yield stress.[10] If small strains are assumed the total strain rate can be additively decomposed into an elastic and a plastic part:

$$\dot{\gamma}^{el}=\mathbf{D}^{-1}\dot{\sigma}, \tag{18}$$

$$\dot{\gamma}^{pl}=\dot{\lambda}\frac{\partial\Phi}{\partial\sigma}. \tag{19}$$

Here, $\dot{\lambda}$ denotes the plastic multiplier which is zero in case of elastic straining and greater than zero in case of plastic straining. To achieve a proper formulation for plasticity eqn (18) and (19) have to be integrated over the loading sequence. Applying a single point integration to the plastic strain rate leads to:

$$\Delta\gamma=\Delta\gamma^{el}+\Delta\gamma^{pl}, \tag{20}$$

$$\Delta\gamma^{el}=\mathbf{D}^{-1}\Delta\sigma, \tag{21}$$

$$\Delta\gamma^{pl}=\Delta\lambda\left.\frac{\partial\Phi}{\partial\sigma}\right|_{t+\alpha\Delta t}, \tag{22}$$

with t denoting the beginning and $t+\alpha\Delta t$ the end of the load step. For every iteration a stress increment $\Delta\sigma$ can be computed by combining eqns (21) and (22) which represents the change of stress while loading:

$$\Delta\sigma=\mathbf{D}\Delta\gamma-\Delta\lambda\mathbf{D}\left.\frac{\partial\Phi}{\partial\sigma}\right|_{t+\alpha\Delta t}. \tag{23}$$

Algorithmically, a trial stress $\sigma_t=\sigma_0+\mathbf{D}\Delta\gamma$ is first computed. If this trial stress does not comply with the yield condition $\Phi(\sigma)\leq 0$ a corrector is applied which returns the stress to the yield surface. Dependent on the choice of the parameter α several methods to compute the stress σ_n can be selected.[11] Here, a fully implicit Euler backward method ($\alpha=1$) is applied. The new stress then equals:

$$\sigma_n=\sigma_0+\Delta\sigma=\sigma_t-\Delta\lambda\mathbf{D}\left.\frac{\partial\Phi}{\partial\sigma}\right|_{t+\Delta t}. \tag{24}$$

This stress has to comply with the yield condition. By substituting eqn (24) into the equation $\Phi(\sigma)=0$ the yield condition is rewritten as function of $\Delta\lambda$. The function $\Phi(\Delta\lambda)$ is solved accomplishing a local Newton–Raphson procedure.

The global iterative procedure is carried out applying finite load steps. For this iterative procedure a tangent stiffness operator must be used which is consistently linearized from eqn (24):

$$\dot{\gamma}^j=\mathbf{D}^{-1}\dot{\sigma}^j+\Delta\lambda^j\frac{\partial^2\Phi}{\partial\sigma^2}\dot{\sigma}^j+\dot{\lambda}\frac{\partial\Phi}{\partial\sigma}. \tag{25}$$

In case of infinitesimal load steps the second term on the right hand side vanishes and leads to the classical continuum elasto-plastic tangent operator. Here finite load steps are considered and omitting the second term leads to a poor convergence behaviour. After some manipulations and using Prager's consistency condition $\dot{\Phi}=0$ the consistent tangent stiffness matrix is derived as:

$$\dot{\sigma}=\left[\mathbf{H}^{-1}-\frac{\mathbf{H}^{-1}\left(\frac{\partial\Phi}{\partial\sigma}\right)\left(\frac{\partial\Phi}{\partial\sigma}\right)^T\mathbf{H}^{-1}}{h+\left(\frac{\partial\Phi}{\partial\sigma}\right)^T\mathbf{H}^{-1}\left(\frac{\partial\Phi}{\partial\sigma}\right)}\right]\dot{\gamma}$$

$$=\mathbf{D}^{con}\dot{\gamma},$$

with h the hardening modulus and

$$\mathbf{H}^{-1}=\mathbf{D}^{-1}+\Delta\lambda\frac{\partial^2\Phi}{\partial\sigma^2},$$

for the von Mises yield criterion. For the Hoffmann criterion a more complicated relation ensures.[12] The derivatives $\partial^2\Phi/\partial\sigma^2$ can be obtained by twice deriving eqns (16) or (17) for the von Mises or the Hoffmann criterion, respectively.

5 NUMERICAL EXAMPLES

5.1 Modelling aspects

For the modelling of layered materials the solid-like shell elements can be applied in two different ways. On the one hand every layer can be modelled individually by an element. This application is advantageous when the interface between the different layers is subject of the investigation. The interface itself can then be represented by special interface elements. On the other hand the element can represent the whole stacking sequence of the layered composite. To achieve this the integration in thickness direction is separated into n_L subintegrations. In this case interlaminar effects cannot be considered.

The material data which is necessary to set up the model must provide information for the whole three-dimensional continuum. In case of isotropic material three material parameters (E, ν, and $\bar{\sigma}$) are employed. Since the prepreg layers are assumed to behave orthotropically, nine elastic and nine plastic parameters are required. The material data are provided for every layer individually. Accordingly, it is possible to apply different models in different layers. This feature is applied when a GLARE® tensile test is computed. Here the yield stresses of the prepreg layers are significantly higher than that of the aluminium layers. Therefore, plasticity is taken into account for the aluminium layers only. For the classical laminate theory this method would lead to the bilinear stress–strain relation. For the orthotropic layers of the buckling examples presented all nine plasticity parameters must be given.

5.2 A square plate under uniform surface load

Firstly, a cross-ply plate as proposed by Kim & Lee[13] is modelled: Fig. 2. The plate is analysed assuming two different stacking sequences: $[90/0]_T$ and $[-45/45]_T$. For the $[90/0]_T$ lay-up one-quarter is modelled with 9 solid-like shell elements. Since the material does not fulfill the symmetry condition the whole structure must be modelled for the $[-45/45]_T$ stacking sequence by employing 36 solid-like shell elements. In thickness direction one element is applied. Since the layers have the same individual thickness, the integration in thickness direction is split into two equal-sized intervals. By defining the characteristic material direction individually per layer the stress–strain relation is obtained layered-wise. The global material parameters are displayed in Table 1 and adopted with respect to the direction chosen in the layer. Here the direction of the fibre orientation is measured with respect to the x-axis of the global frame of reference, Fig. 2. The edges of the plate are clamped. The plate is subjected to a uniform surface load of 1·0 psi. In this case only geometrically nonlinear behaviour is taken into account. The force is applied performing three equal-sized load steps with an initial load parameter $\Delta\lambda=0{\cdot}5$. The results of the calculations are displayed in Fig. 3. Obviously, the results obtained with thick shell elements agree well with those computed by applying standard elements in the calculation of Kim & Lee.[13]

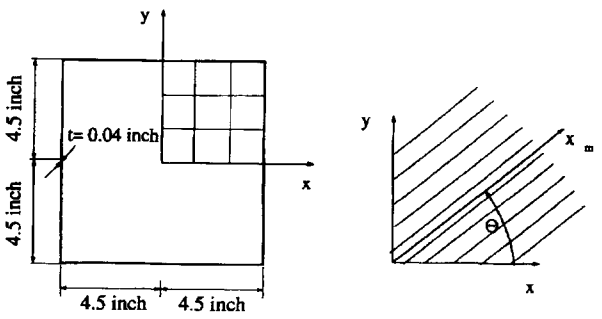

Fig. 2. Geometry of the plate under surface loading as proposed by Kim & Lee.

Table 1. Elastic material parameters for the orthotropic plate as proposed by Kim & Lee

Young (psi)	Shear (psi)	Poisson
E_{11} $2{\cdot}0\times10^{+7}$	G_{12} $7{\cdot}0\times10^{+5}$	ν_{12} 0·3
E_{22} $1{\cdot}4\times10^{+6}$	G_{23} $7{\cdot}0\times10^{+5}$	ν_{23} 0·3
E_{33} $1{\cdot}4\times10^{+6}$	G_{13} $7{\cdot}0\times10^{+5}$	ν_{13} 0·3

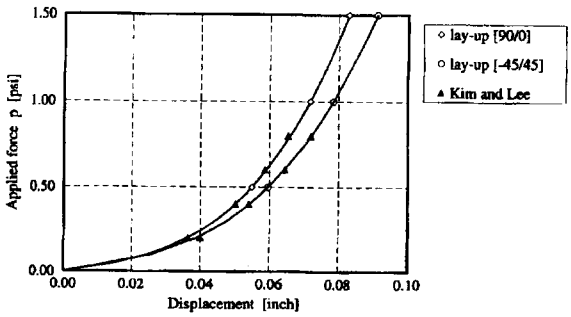

Fig. 3. Load displacement curve of the center of the orthotropic plate as proposed by Kim & Lee.

5.3 A square plate under compressive loading

The same plate is loaded with a compressive in-plane load, Fig. 4. In order to obtain buckling behaviour a double sinusoidal out of plane imperfection is introduced. In the initial state the amplitude of the imperfection equals 0·001 inch in the middle of the plate. The $[90/0]_T$ lay-up is examined and a clamped as well as a hinged configuration are calculated. These boundary conditions are applied to the edges on which the load acts. The other edges remain free. In the clamped case the displacements in the x-direction and z-direction are zero. In the y-direction the nodes at the boundary may displace with the same value. In the hinged configuration the displacements in the y-direction of the top nodes are equal to each other. For the bottom nodes a similar relation holds. The plate is modelled using 5 elements in loading direction and 3 elements perpendicular to the loading direction. The analysis is performed applying an arc-length control procedure with a reference load of $p=25000$ lbs/inch.[2] The results are exposed in Fig. 5. Obviously, they show a good agreement with results obtained by Schellekens.[12] It can be seen in Fig. 5 that the clamped plate has a higher load capacity. In the clamped configuration the critical buckling load is four times higher than the buckling load in the hinged configuration. Since the buckling length of the hinged configuration is twice as large as the buckling length in the clamped configuration this result is expected.

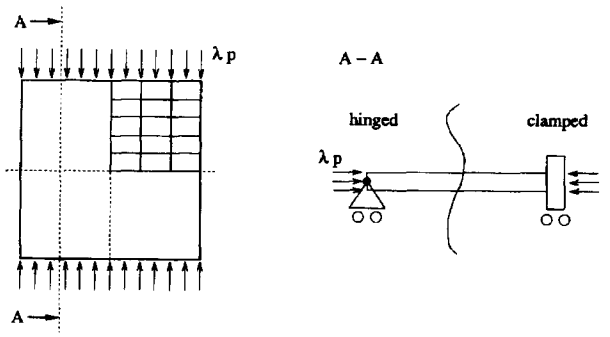

Fig. 4. Geometry and boundary conditions of the square plate under compressive loading.

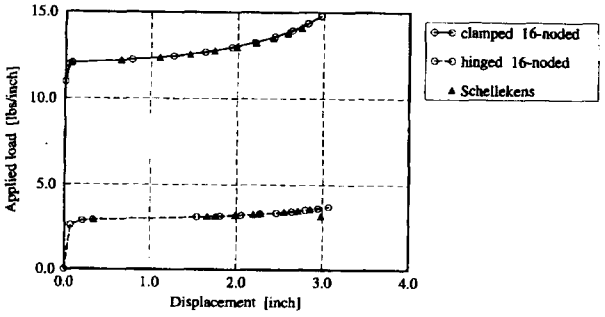

Fig. 5. Load deflection curve for the center of the square plate under compressive loading.

5.4 Analysis of a plate under compressive loading

Since in the previous example the geometrically nonlinear behaviour of the elements has been subject of the calculations the following example includes physically nonlinear behaviour. The example consists of a plate which is loaded by a compressive force at two opposite edges of the plate.[14] One quarter of the plate is modelled with 32 solid-like shell elements. The plate is simply supported at the edges where the load is applied. A double sinusoidal variation of the thickness introduces the imperfection to obtain buckling behaviour. The amplitude of this imperfection equals 0·294 mm whereby the thickness of the plate is $t=6{\cdot}00$ mm. The other geometrical properties are given in Fig. 6. The magnitude of the pressure equals 87·46 N/mm^2 which is related to the critical buckling force P_{cr} for this plate.[14] Two material configurations have been investigated: in the first example a purely isotropic material is applied and in the second case an orthotropic material is selected. The material parameters of the isotropic material equal: $E=210{\cdot}0$ kN/mm^2, $\nu=0{\cdot}3$. For this material the von Mises yield criterion is adopted with a yield value $\sigma_y=240{\cdot}0$ N/mm^2. The anisotropic configuration consists of three layers composed of uniaxial orthotropic material: $[90]_T$, where the angle is measured with respect to the x-axis, Fig. 6. The elastic material parameters and the plastic material parameters are

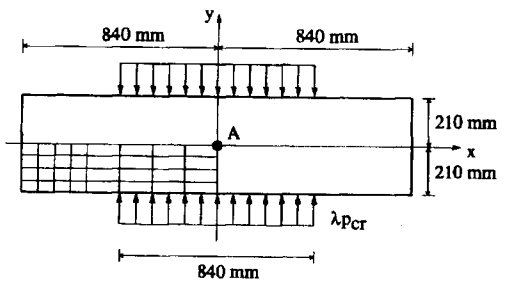

Fig. 6. Plate subjected to compressive loading as proposed by Ramm.

Table 2. Elastic material parameters for the plate proposed by Ramm assuming anisotropic material

Young (MPa)	Shear (MPa)	Poisson
E_{11} 180·0 × 10^{+3}	G_{12} 7·0 × 10^{+3}	ν_{12} 0·28
E_{22} 60·0 × 10^{+3}	G_{23} 7·0 × 10^{+3}	ν_{23} 0·28
E_{33} 60·0 × 10^{+3}	G_{13} 7·0 × 10^{+3}	ν_{13} 0·28

Table 3. Plastic material parameters for the plate proposed by Ramm assuming anisotropic material

	Tension (MPa)	Compression (MPa)		Shear (MPa)
$\bar{\sigma}^{11}$	200·0	150·0	$\bar{\sigma}_{44}$	70·0
$\bar{\sigma}^{22}$	40·0	50·0	$\bar{\sigma}_{55}$	70·0
$\bar{\sigma}^{33}$	40·0	50·0	$\bar{\sigma}_{66}$	70·0

given in Table 2 and Table 3, respectively. The reference load is applied using an arc-length control procedure.[6] To calculate the stiffness matrices a 2 × 2 Gauss-integration is applied on the surface. In thickness direction the integration is accomplished using a different number of integration points (two up to seven).

The comparison for the center deflection of the isotropic case is shown in Fig. 7. The calculations with solid-like shell elements result in the same reaction compared with the results obtained by standard shell elements.[11] Applying standard shell elements in this benchmark test a 7-point integration in thickness direction is required to obtain sufficient results, while a 4-point integration leads to sufficient results for the solid-like shell element.

The results obtained with solid-like shell elements in the orthotropic case show good agreement with the results using standard shell elements, Fig. 8. Hereby the calculations are performed with 2 integration points per layer. However, it is emphasized that differences between both simulations may occur especially if the boundary conditions cause different effects in the solid-like shell element compared to the standard shell elements which are governed by a plane stress or plane strain assumption. A conclusion of this benchmark test and other tests carried out[5] is that the solid-like shell element is well suited for modelling the behaviour of laminated structures.

5.5 GLARE® tensile test

A GLARE® tensile test is now simulated using solid-like shell elements. The test has been performed at the Production and Materials Laboratory of the Faculty of Aeronautical Engineering of Delft University of Technology[15] in the framework of a collaborative research project on fibre metal laminates. The test configuration is displayed in Fig. 9. One quarter of the specimen is modelled using either 40 elements or 200 elements. In the case of 40 elements each element represents the whole stacking sequence. Applying 200 element each element acts in one material layer. The elements are connected in thickness direction. As Young's modulus of the aluminium layer E=72000 MPa and as Poisson number ν=0·33 are adopted. To assess the effects of temperature variation a thermal expansion coefficient

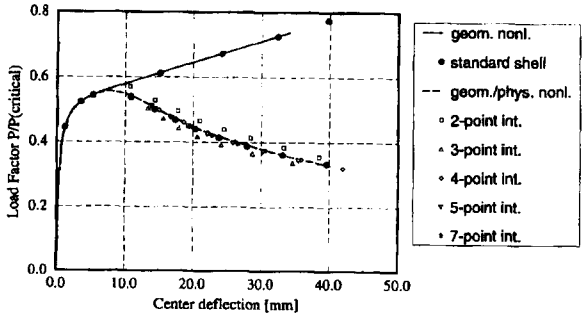

Fig. 7. Load deflection curve for the center of the compressed plate assuming isotropic material behaviour.

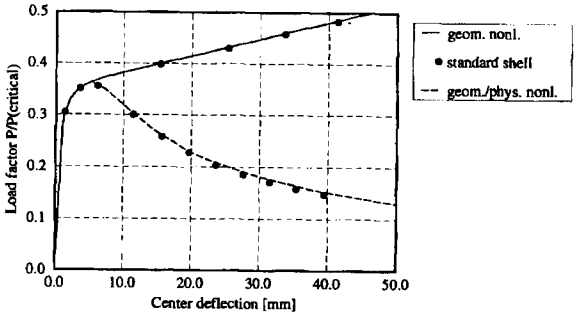

Fig. 8. Load deflection curve for the center of the compressed plate assuming orthotropic material: $[90]_T$.

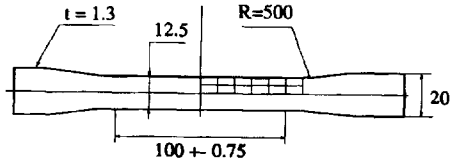

Fig. 9. Test specimen of the GLARE® tensile test in mm.

Table 4. Elastic material parameters for the GLARE® prepreg layer

Orthotropic layer			
Young (MPa)	Shear (MPa)	Poisson	Them. expand. coef. (1/K)
E_{11} 53980·0	G_{12} 5548·0	ν_{12} 0·33	α_{11} $6{\cdot}1\times10^{-6}$
E_{22} 9412·0	G_{23} 5548·0	ν_{23} 0·0575	α_{22} $2{\cdot}6\times10^{-5}$
E_{33} 9412·0	G_{13} 5548·0	ν_{13} 0·0575	α_{33} $2{\cdot}6\times10^{-5}$

$\alpha=2{\cdot}3\times10^{-5}$ $1/K$ is used. The yield value of the aluminium layer equals $\bar{\sigma}=310$ N/mm^2. Since the plastic parameters of the R-Glass prepreg are significantly higher than those of aluminium plasticity is not taken into account for the prepreg. The elastic material parameters for the prepreg layers are collected in Table 4. While producing ARALL® and GLARE® the aluminium layers are connected to the prepreg layers at a temperature $T_{Prod}=393$ K. The test however is carried out at a temperature $T_{Exp}=293$ K. The resulting initial stress is accounted for by simulating the cooling before loading the test specimen. The material is assumed to behave geometrically linear whereby the aluminium layer is governed by the von Mises yield criterion. In one of the calculations hardening of the aluminium layer is assumed. The hardening parameter expected for the aluminium layer is taken from Ramm.[16]

The results are shown in Fig. 10. Here the strain is computed as end displacement related to the initial length after cooling. The stress is computed as applied force related to the gross area in the configuration after cooling which does not significantly differ from the gross area before cooling. No significant difference in the strain–stress diagram between the model using 200 elements and the model using 40 elements could be noticed. All simulations show good agreement with the experimental data. Especially the calculations incorporating hardening lead to good agreement with the experimental behaviour. In the latter case the slope of the curve follows the experimentally obtained curve. If no hardening is assumed the difference between the experimental data and the numerical data increases with increasing strains. Since aluminium in general shows a typical hardening behaviour this effect could be expected. The impact of the temperature drop on the results is minor in this case.

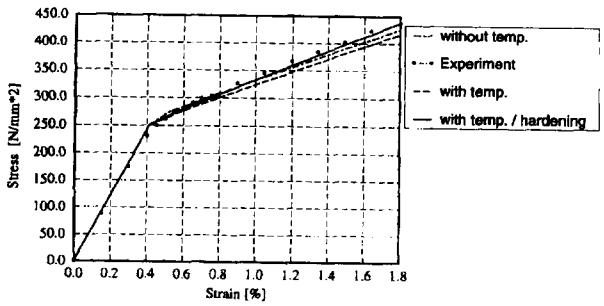

Fig. 10. Finite element simulation of a GLARE® specimen in a tensile test.

6 CONCLUSIONS

The paper introduces the concept of a solid-like shell element and its application for modelling fibre metal laminates. As a first step it has been proved that the solid-like shell element applied here leads to the same results obtained using standard shell elements for a theoretical benchmark test. Subsequently, the element has been employed to model an experiment using GLARE®. The comparisons show a good agreement between the numerical and experimental results. Therefore these solid-like shell elements are suitable for the calculation of the behaviour of laminated structures.

REFERENCES

1. Akzo Fibers, *Technical Information Aerospace ARALL and GLARE®*, Product Information Brochure, Akzo Fibres and Polymer Division, 1990.
2. Simo, J. C., Rifai, M. S. & Fox, D. D., On a stress resultant geometrically exact shell model. Part IV: variable thickness shells with through-the-thickness stretching. *Comp. Meth. Appl. Mech. Engng*, **81** (1990) 91–126.
3. Büchter, N., Ramm, E. & Roehl, D., Three-dimensional extension of nonlinear shell formulation based on the enhanced assumed strain concept. In *Computational Methods in Applied Science*, eds Ch. Hirsch, J.

Periaux, J. & Oñate, E., Elsevier, Oxford, 1992.
4. Parisch, H., A continuum-based shell theory for non-linear applications. *Int. J. Num. Meth. Engng*, **38**, 1995, 1855–83.
5. Hashagen, F., A geometrically and physically nonlinear layered thick shell element. *TU-Delft Report*, nr. 03-21-0-31-22, Delft University of Technology, 1995.
6. Feenstra, P. H. & Schellekens, J. C. J., Self-adaptive solution algorithm for a constrained Newton-Raphson method. *TU-Delft Report nr. 25.2-91-2-13*, Delft University of Technology, 1991.
7. de Borst, R. & Feenstra, P. H., Studies in anisotropic plasticity with reference to the Hill criterion. *Int. J. Num. Meth. Engng*, **29** (1990) 325–36.
8. Hoffmann, O., The brittle strength of orthotropic materials. *J. Comp. Mat.*, **1** (1986) 200–6.
9. Hill, R., A theory of the yielding and plastic flow of anisotropic materials. In *Proc. R. Soc.*, **A193**, 1947, pp. 281–97.
10. Schellekens, J. C. J. & de Borst, R., The use of the Hoffmann yield criterion in finite element analysis of anisotropic composites. *Computers & Struct.*, **37** (1990) 1087–96.
11. Crisfield, M. A., *Non-linear Finite Element Analysis of Solids and Structures*, Vol. I, Wiley Publishers, NY, 1991, pp. 252–335.
12. Schellekens, J. C. J., A geometrically and physically nonlinear layered shell element. *TU-Delft Report nr. 25-2-91-2-12*, Delft University of Technology, 1991.
13. Kim, Y. H. & Lee, S. W., A solid element formulation for large deflection analysis of composite shell structures. *Computers & Struct.*, **30** (1988) 269–70.
14. Ramm, E., Strategies for tracing the nonlinear response near limit points. In *Nonlinear Finite Element Analysis in Structural Mechanics*, eds. W. Wunderlich *et al.*, Springer Verlag, Berlin, 1981, pp. 63–89.
15. de Vries, T., Various parameters concerning the residual strength of aircraft materials, Part II, test data and charts, MSc thesis, Delft University of Technology, 1994.
16. Ramm, E. & Matzenmiller, A., Computational aspects of elasto-plasticity in shell analysis. In *Proc. Int. Conf. Computational Plasticity*, eds D. R. J. Owen, E. Hinton & E. Oñate. Pineridge Press, Swansea, 1987, pp. 711–35.